Optimal Sampling of Dynamical Large Deviations in Two Dimensions via Tensor Networks

Luke Causer,[1,2] Mari Carmen Bañuls,[3,4] and Juan P. Garrahan[1,2]
[1]School of Physics and Astronomy, University of Nottingham, Nottingham, NG7 2RD, United Kingdom
[2]Centre for the Mathematics and Theoretical Physics of Quantum Non-Equilibrium Systems, University of Nottingham, Nottingham, NG7 2RD, United Kingdom
[3]Max-Planck-Institut für Quantenoptik, Hans-Kopfermann-Str. 1, D-85748 Garching, Germany
[4]Munich Center for Quantum Science and Technology (MCQST), Schellingstr. 4, D-80799 München

(Received 17 October 2022; accepted 20 March 2023; published 4 April 2023)

We use projected entangled-pair states (PEPS) to calculate the large deviation statistics of the dynamical activity of the two-dimensional East model, and the two-dimensional symmetric simple exclusion process (SSEP) with open boundaries, in lattices of up to 40×40 sites. We show that at long times both models have phase transitions between active and inactive dynamical phases. For the 2D East model we find that this trajectory transition is of the first order, while for the SSEP we find indications of a second order transition. We then show how the PEPS can be used to implement a trajectory sampling scheme capable of directly accessing rare trajectories. We also discuss how the methods described here can be extended to study rare events at finite times.

DOI: 10.1103/PhysRevLett.130.147401

Introduction.—Tensor network (TN) techniques, whereas most actively developed in the context of quantum many-body physics [1–6], offer powerful numerical tools for much more general problems. They are based on an efficient parametrization of the many-body state in terms of local tensors (multidimensional arrays) connected according to a graph that, in general, responds to the structure of correlations in the state. In the last few years we have seen progress in their application to compute statistical properties of dynamical trajectories in classical stochastic systems. The first application was to the long time statistics—the dynamical large deviation (LD) regime—of one-dimensional lattice systems using variational algorithms (such as density matrix renormalization group [7], or DMRG) to approximate the leading eigenvectors of tilted Markov generators by matrix product states (or MPS, see, e.g., Ref. [2]) [8–15]. Building on these results, we recently introduced (i) a method which exploited MPS to efficiently sample long-time rare trajectories, and (ii) an MPS time evolution to precisely compute trajectory statistics at finite times [16].

The suitability of the TN ansatz for these problems is rooted in the fact that the targeted eigenvectors have low correlations. More concretely, for local problems, we expect them to fulfill (up to small corrections) a so-called area law [17], according to which the "entanglement" (or a mathematically analogous quantity for classical probability vectors [18]) with respect to a bipartition is upper bounded by the size of its boundary. This scaling is captured by the MPS family in one spatial dimension. In higher dimensions, a suitable generalization with area law is provided by the projected-entangled pair states (PEPS) [19], which were recently applied to the classical asymmetric exclusion process in two dimensions in Ref. [20]. A computationally cheaper alternative, without an area law but accommodating more entanglement than MPS, is that of tree tensor networks [21], used, for example, in Refs. [22,23] (in combination with a time-dependent variational principle [24]) to study driven problems.

Here we use PEPS to study the LDs of the *dynamical activity* in two paradigmatic two-dimensional models, the 2D East model (also known as North-or-East model) [25–28], and the 2D symmetric simple exclusion process (SSEP) with open boundaries where particles can be injected and removed [29]. We are able to accurately estimate the leading eigenvector of the tilted generator—and thus the LDs—of these models, and construct a close-to-optimal dynamics to directly sample the corresponding rare trajectories. Such an algorithm requires efficient sampling from the PEPS, and we show how to do this in the context of trajectory sampling. We benchmark our methods, showing how the PEPS allows for a controlled accuracy of optimal dynamics. We demonstrate that both models have a phase transition between active and inactive dynamical phases, a first-order transition for the 2D East and a second-order transition for the 2D SSEP.

Published by the American Physical Society under the terms of the Creative Commons Attribution 4.0 International license. Further distribution of this work must maintain attribution to the author(s) and the published article's title, journal citation, and DOI.

Models.—The models we study here live in a two-dimensional square lattice of size $N = L \times L$, with each site being occupied by a binary variable $n_{\boldsymbol{k}} = 0$ or 1, where $\boldsymbol{k} = (k_x, k_y)$ denotes the position of the site for $k_x, k_y = 1 \cdots L$. Their continuous-time dynamics is defined by a Markov generator (e.g., see Refs. [35,36]),

$$\mathbb{W} = \sum_{x, y \neq x} w_{x \to y} |y\rangle\langle x| - \sum_x R_x |x\rangle\langle x|, \tag{1}$$

where $|x\rangle$ and $|y\rangle$ are configurations on the lattice, $w_{x\to y}$ the transition rate from x to y, and $R_x = \sum_{y\neq x} w_{x\to y}$ the escape rate out of x. We can write this as $\mathbb{W} = \mathbb{K} - \mathbb{R}$, where $\mathbb{K}$ contains the off-diagonal transition rates, and $\mathbb{R}$ the diagonal escape rates.

The first model we consider is the 2D East model [25–28], often studied in the context of the glass transition. This is a kinetically constrained model such that an excited site $n_{\boldsymbol{k}} = 1$, allows ("facilitates") a site to its North or East to flip stochastically, see Fig. 1(a). It is parametrized by $c \in (0, 1/2]$, which determines the local transitions rates: $0 \to 1$ with rate c, and $1 \to 0$ with rate $1 - c$, subject to the kinetic constraint. In addition, we choose open boundary conditions with $n_{(1,1)} = 1$ fixed. This ensures the entire state space remains dynamically connected [26]. The second model is the 2D SSEP. This describes particles hopping to neighboring sites on a 2D lattice with unit rate, but only if the target site is not already occupied by a particle. We also allow particles to be injected or removed at the boundaries of the lattice with rate $1/2$, see Fig. 1(b). Exact definitions of the models are given in Ref. [30].

Dynamical large deviations.—We consider the statistics of a dynamical observable $\hat{K}$ through its probability distribution $P_t(K) = \sum_{\omega_t} \pi(\omega_t)\delta[\hat{K}(\omega_t) - K]$, where ω_t denotes a stochastic trajectory and $\pi(\omega_t)$ its probability. The corresponding moment generating function is $Z_t(s) = \sum_{\omega_t} \pi(\omega_t) e^{-s\hat{K}(\omega_t)}$. In the $t \to \infty$ limit, the two obey LD principles $P_t(K) \asymp e^{-t\varphi(K/t)}$ and $Z_t(s) \asymp e^{t\theta(s)}$, with the rate function $\varphi(K/t)$ and scaled cumulant generating function (SCGF) $\theta(s)$ related through a Legendre transform, $\theta(s) = -\min_k[sk + \varphi(k)]$ for $k = K/t$ (for reviews see Refs. [36–39]).

We focus as an observable on the *dynamical activity* [40,41], which counts the number of jumps in a trajectory. The relevant operator to study is the *tilted generator* [36–39], which for the activity reads $\mathbb{W}_s = e^{-s}\mathbb{K} - \mathbb{R}$, with the LD statistics encoded in the leading eigenvalue and (right and left) eigenvector(s), $\mathbb{W}_s|r_s\rangle = \theta(s)|r_s\rangle$ and $\langle l_s|\mathbb{W}_s = \theta(s)\langle l_s|$.

Projected-entangled pair states.—TN methods allow us to solve the problem above using a variational ansatz for $|\psi_s\rangle$ in the PEPS family, a natural generalization of MPS for area law states and lattices in more than one spatial dimension [19]. PEPS parametrize the many-body state

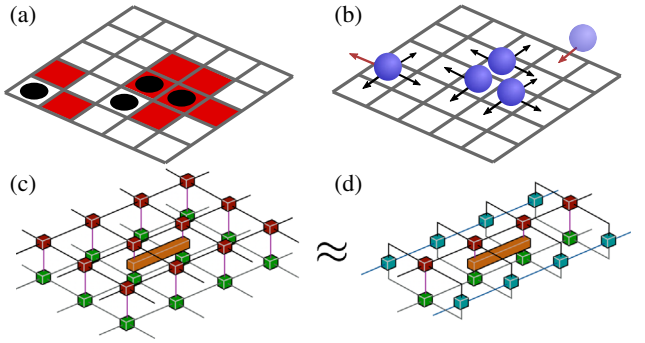

FIG. 1. Models. (a) 2D East: an occupied site (black circles) facilitates flips in neighboring sites (red cells) only in two directions. (b) 2D SSEP: particles can hop to empty neighboring sites (black arrows), symmetrically in any direction; particles can enter or leave at the boundaries (red arrows). PEPS. (c) A PEPS is parametrized by a tensor per lattice site (red boxes for the top PEPS), each local tensor with a physical index (purple line) and four virtual legs (black lines) that connect it to neighboring tensors. The expectation value of a local operator (orange box) is obtained by sandwiching it between the PEPS and its adjoint (shown in green), and contracting (i.e., multiplying and summing over) the physical (basis) indices. (d) The cost of exact contraction scales exponentially with size, so an MPS approximation (blue tensors) is used for the contraction part of the network, with the dimension of its virtual bonds (blue legs) controlling accuracy; see Ref. [30] for details.

with one rank-5 tensor per lattice site, in which the *physical* index has the dimension of the site variable (0, 1 in our case), and the remaining four *virtual* indices each have bond dimension D_{PEPS}, determining the maximum number of parameters in the ansatz, $N_p = NdD^4_{\text{PEPS}}$ (see Fig. 1 for a graphical representation). Several TN algorithms exist to optimize the PEPS by maximizing the expectation of a local stochastic generator. Crucial to all of them is an efficient computation of expectation values for local operators, such as the terms in $\mathbb{W}_s$. We use the boundary MPS scheme [1,19] (illustrated in Fig. 1), which approximates the partial contraction of the network by a MPS, whose bond dimension χ_B controls the accuracy of the contraction. A heuristic choice for local problems is $\chi_B \sim O(D^2_{\text{PEPS}})$ (see, e.g., Ref. [42]).

In order to find the PEPS approximation to the leading eigenvector $|\psi_s\rangle$ we employ time evolution, which effectively projects the ansatz onto the leading eigenvector by iteratively applying short evolution steps, decomposed in two-body terms that are applied sequentially [6,43]. After each operation, the directly affected pair of tensors is updated. This requires a strategy to approximate their environment (i.e., the contraction of the remaining TN). After comparing to quasi-exact [44] results and to a more expensive strategy, we find that the computationally cheapest simple update (SU) [45], with maximal PEPS bond dimension $D_{\text{PEPS}} = 4$, is enough to achieve sufficiently accurate measurements of the SCGF in our problems, and

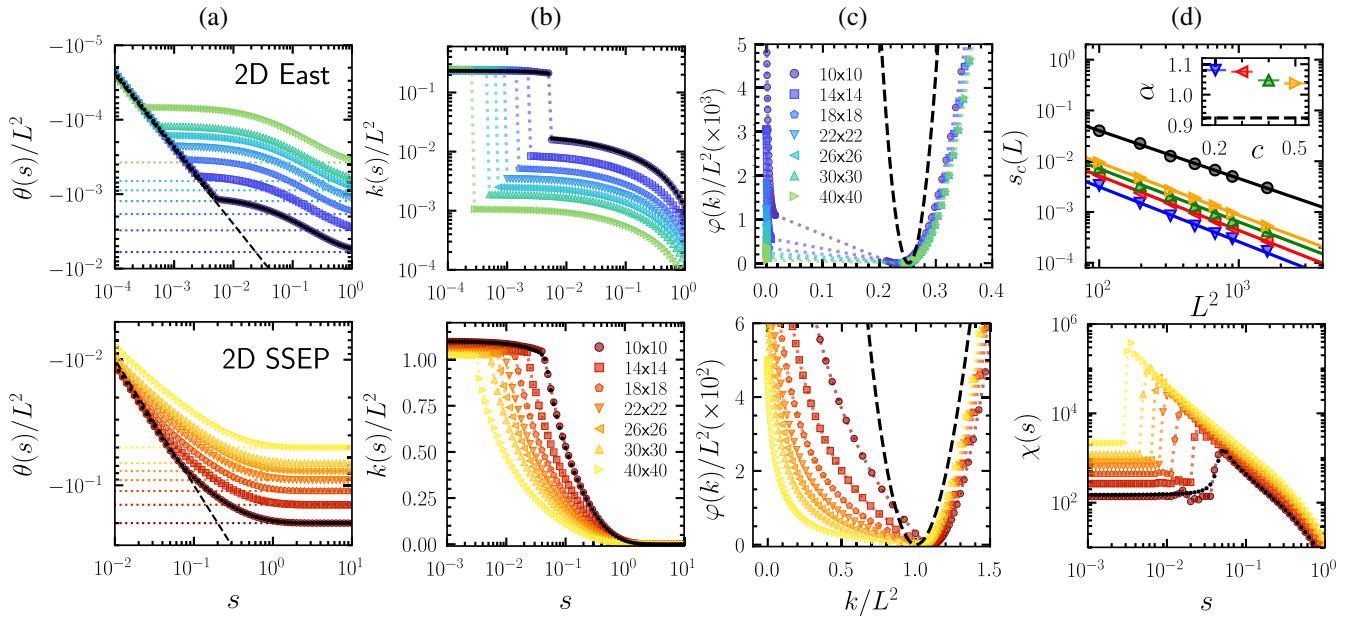

FIG. 2. Dynamical large deviations and active-inactive transitions from PEPS. (a) The SCGF $\theta(s)/L^2$ for the 2D East with $c = 0.3$ (top) and the SSEP (bottom) for system sizes $N \in [10^2, 40^2]$. The black dashed line shows the linear response for small s, and the color dotted lines show the value for $s \to \infty$. (b) The dynamical activity $k(s)/L^2$ for the systems in (a). The East is on a log-log scale, and the SSEP a log-linear scale. (c) The rate function $\varphi(k)/L^2$ as a function of activity k/L^2 for the systems in (a). The dashed line shows the Poisson distribution with mean $k(s=0)/L^2$. (d) The transition points $s_c(L)$ for the 2D SSEP (black circles) and the 2D East for $c \in [0.2, 0.5]$. The solid lines show the fitted power-law curves $s_c(L) \sim L^{-2\alpha}$, with the exponents shown in the inset. The black dashed line is the exponent for the SSEP, and the symbols are for the East. The symbols can be used to read the value of c in the main figure. The bottom panel shows the dynamical susceptibility $\chi(s) = \theta''(s)$ for the 2D SSEP. All the data was acquired using the SU except for the black markers, which show (quasi-exact) 2D DMRG data for a $N = 10$ lattice for comparison.

allows us reaching large sizes at low computational cost, scaling only as $O(D^5_{\mathrm{PEPS}})$. For further details on the numerical approach we use see Ref. [30].

Large deviations from PEPS.—The East and SSEP in one dimension are known to have dynamical phase transitions in terms of the activity or other dynamical observables [11,13,40,46–53]. In two dimensions, the SSEP has a transition in the LDs of the current [20]. We now provide evidence by means of PEPS for both the 2D East and 2D SSEP having active-inactive phase transitions. Figures 2(a)–2(c) show the LD statistics for both the 2D East model (top) and the 2D SSEP (bottom). For the East model, we see from Fig. 2(a) that the SCGF follows a linear response, $\theta(s) \approx sk(0)$, for small s, but at $s_c(L)$ it sharply changes to another branch. This point corresponds to a sudden drop in activity, $k(s) = -\theta'(s)$, which becomes discontinuous in the limit $N \to \infty$, see Fig. 2(b). Having access to both the SCGF and the dynamical activity allows us to estimate the rate function $\varphi(k)$, shown in Fig. 2(c). We see a broadening of the rate function around the mean, indicating the coexistence of active and inactive dynamics. For comparison, we also show the distribution of a simple process with the same mean activity, but which is uncorrelated in time (black dashed line). All this behavior is characteristic of a first-order phase transition.

For the SSEP we see something different: Fig. 2(a) shows no sharp change in $\theta(s)$, and the activity in Fig. 2(b) has no discontinuity. This is indicative of a second-order transition, with the rate function showing critical broadening, see Fig. 2(c), and a divergence in the susceptibility $\chi(s) = \theta''(s)$, see Fig. 2(d). For both models we can extract a transition point from the drop in either first or second cumulant. The top panel of Fig. 2(d) shows how the transition point scales with L for both models (for a range of c for the 2D East). We are able to fit the data with the power laws $s_c(L) \sim L^{-2\alpha}$, as shown by the solid lines. We find the exponents $\alpha \gtrsim 1$ for the 2D East and $\alpha \lesssim 1$ for the SSEP, see the inset to the top panel of Fig. 2(d).

Optimal sampling of rare trajectories from PEPS.—Sampling trajectories corresponding to the $s \neq 0$ phases is difficult as they are exponentially rare in system size and time. The optimal sampling dynamics at long times is given by the so-called *generalized Doob transform* [55–59], which maps the tilted generator into a true stochastic generator for the rare trajectories, $\mathbb{W}_s^{\mathrm{Doob}} = \mathbb{L}[\mathbb{W}_s - \theta(s)\mathbb{I}]\mathbb{L}^{-1}$, where $\mathbb{L}$ is the leading left eigenvector of $\mathbb{W}_s$ as a diagonal matrix. This gives a new dynamics with the transition rates

$$\tilde{w}_{x\to y} = \frac{l_s(y)}{l_s(x)} e^{-s} w_{x\to y}, \tag{2}$$

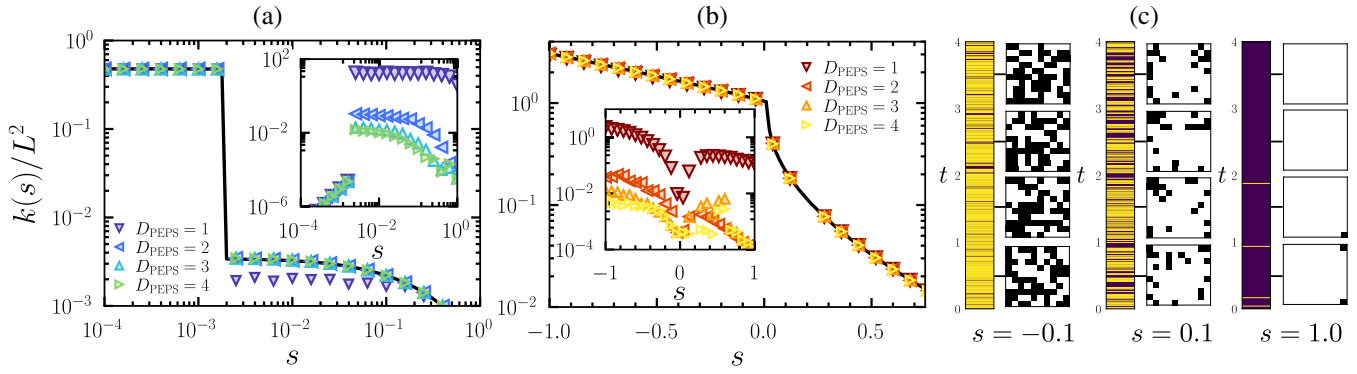

FIG. 3. Optimal sampling of trajectories. (a) Average dynamical activity as a function of s for the 2D East model from CTMC with importance sampling (symbols), for $c = 0.5$ and $D_{\mathrm{PEPS}} \in [1, 4]$. The trajectory times are chosen such that on average we expect 100 transitions per trajectory. The solid black line shows the activity measured directly from the PEPS with $D = 4$ for comparison. Inset: variance in the time-integrated difference of escape rates, δR^2 (see main text). Each data point is calculated from $N_{\mathrm{sp}} \in [10^3, 10^4]$ trajectories. (b) Same but for the 2D SSEP on a 22×22 lattice. (c) Representative trajectories for the 2D SSEP for size $N = 10 \times 10$ at three values of $s \neq 0$. The bars on the left of each panel show the times when particle hops occur (yellow and bright lines). The snapshots on the right show the configurations at the marked times (black or white indicates a particle or hole). See also Refs. [30,54].

with $l_s(x) = \langle l_s|x\rangle$. In $\mathbb{W}_s^{\mathrm{Doob}}$ the counting field s appears as a physical control parameter, and running dynamics with rates (2) gives trajectories at $s \neq 0$ on demand. While optimal, $\mathbb{W}_s^{\mathrm{Doob}}$ is difficult to construct in general as one needs the exact left leading eigenvector. However, we can exploit our PEPS approximation to estimate the rates Eq. (2), similar to Ref. [60] for 1D and MPS, see Ref. [30] for more information.

To obtain Eq. (2) for the transitions out of a state x we calculate $l_s(y)$ from the PEPS using a boundary dimension $\chi_B = D_{\mathrm{PEPS}}$ [61–64], thus entailing a maximum cost $O(ND_{\mathrm{PEPS}}^6)$. If we neglect the time edges of trajectories, we can estimate an time-extensive observable by importance sampling

$$\langle O\rangle_s \approx \frac{\sum_{\alpha_t} O(\alpha_t) g(\alpha_t)}{\sum_{\alpha_t} g(\alpha_t)}, \tag{3}$$

where α_t denotes a trajectory generated with Eq. (2) (the *reference dynamics*), and $O(\alpha_t)$ is the trajectory observable. The reweighting factor $g(\alpha_t)$ is

$$g(\omega_t) = e^{-\int_0^t dt' R(t') - \tilde{R}(t')}, \tag{4}$$

where $R(t')$ and $\tilde{R}(t')$ are the escape rates of the system at time t' in the original dynamics and the approximate Doob dynamics, respectively. Notice that with a large enough number of trajectories, Eq. (3) can be used to correct on the imperfections in the reference dynamics due to an imperfect PEPS approximation.

Figure 3 shows results from our sampling algorithm for the 2D East with $c = 0.5$ and the 2D SSEP, both for system sizes $N = 22 \times 22$. The average dynamical activity measured in trajectories (symbols) [with umbrella sampling Eqs. (3), (4)] coincides with that obtained directly from the PEPS (solid line), except for $D_{\mathrm{PEPS}} = 1$ for the East model. The accuracy of our dynamics is quantified by the variance of the time integrated difference in escape rates, cf. Eq. (4), which vanishes for the exact Doob rates. We show this for each D in the insets of Figs. 3: increasing the D_{PEPS} consistently reduces the variance, indicating a better sampling dynamics and less need for importance sampling.

The PEPS approximation to the leading eigenvalue gives us direct access to the long time-averaged properties of the dynamics. However, the broader range of dynamical information—such as temporal correlations—can only be obtained through the simulation of the dynamics in rare dynamical regimes. The ability to exploiting the PEPS to define an efficient trajectory sampling scheme for the biased dynamics allows us to characterize the finite-time atypical behavior beyond what is directly encoded in the PEPS approximation. Figure 3(c) illustrates this by showing sample trajectories for the SSEP at $s \neq 0$: in the active phase ($s = -0.1$ panel), particle hops are plentiful, as shown in the bar on the left of the panel, and the configurations visited in the trajectory have a finite density and show no appreciable clustering; in contrast in the inactive phase ($s = 1.0$ panel), hops are scarce and the configurations have very low density of particles; near the transition ($s = 0.1$ panel), configurations show more pronounced density fluctuations, related to the critical nature of the transition.

Discussion.—We have shown that the dynamical LDs of two-dimensional stochastic models can be studied efficiently with PEPS, including the quasi-optimal sampling of atypical trajectories. Compared to more standard methods [65–71], PEPS offer the advantage of a computational cost that scales only polynomially in the system size and the tensor dimensions D_{PEPS}. Furthermore, the algorithms

produce an explicit ansatz for the leading eigenvector encoding the LDs, which allows us to extract all (local) observables in the biased trajectory ensemble and, as shown above, to devise a near-to-optimal sampling dynamics. Additionally, because PEPS form a complete family, by increasing the bond dimension the quality of the solution can be systematically improved, a property that can also be utilized to estimate the error of the approximation. Our results show that the PEPS ansatz is well suited for these problems, as a moderate bond dimension suffices to explore large systems.

We showed here that both the 2D East model and the 2D SSEP have active-inactive trajectory transitions, of the first-order and second-order, respectively. Our Letter adds to the continuously expanding application [8–16,20,22,23,72] of tensor network methods to study the dynamical fluctuations in classical stochastic systems.

There are several interesting avenues to pursue building on this Letter. One is to integrate 2D trajectory sampling via TNs with a method such as transition path sampling [73] for investigating statistics of fluctuations at *finite times*, cf. Refs. [16,74]. While the current implementations with PEPS are too demanding to reasonably incorporate transition path sampling, tree tensor networks [21] are a promising alternative that could allow to reliably investigate finite time scaling. We hope to report on this is the near future.

We acknowledge financial support from EPSRC Grant No. EP/R04421X/1 and the Leverhulme Trust Grant No. RPG-2018-181. M. C. B. acknowledges support from Deutsche Forschungsgemeinschaft (DFG, German Research Foundation) under Germany's Excellence Strategy—EXC-2111–390814868. Calculations were performed using the Sulis Tier 2 HPC platform hosted by the Scientific Computing Research Technology Platform at the University of Warwick. Sulis is funded by EPSRC Grant EP/T022108/1 and the HPC Midlands + consortium. We acknowledge access to the University of Nottingham Augusta HPC service. Example code used to generate the data can be found at https://github.com/lcauser/2d-optimal-sampling. Data is available at Ref. [54].

[1] F. Verstraete, V. Murg, and J. Cirac, Adv. Phys. **57**, 143 (2008).
[2] U. Schollwöck, Ann. Phys. (Amsterdam) **326**, 96 (2011).
[3] R. Orús, Ann. Phys. (Amsterdam) **349**, 117 (2014).
[4] P. Silvi, F. Tschirsich, M. Gerster, J. Jünemann, D. Jaschke, M. Rizzi, and S. Montangero, SciPost Phys. Lect. Notes **8** (2019).10.21468/SciPostPhysLectNotes.8
[5] K. Okunishi, T. Nishino, and H. Ueda, J. Phys. Soc. Jpn. **91**, 062001 (2022).
[6] M. C. Bañuls, Annu. Rev. Condens. Matter Phys. **14**, 173 (2023).
[7] S. R. White, Phys. Rev. Lett. **69**, 2863 (1992).
[8] M. Gorissen, J. Hooyberghs, and C. Vanderzande, Phys. Rev. E **79**, 020101(R) (2009).
[9] M. Gorissen and C. Vanderzande, Phys. Rev. E **86**, 051114 (2012).
[10] M. Gorissen, A. Lazarescu, K. Mallick, and C. Vanderzande, Phys. Rev. Lett. **109**, 170601 (2012).
[11] M. C. Bañuls and J. P. Garrahan, Phys. Rev. Lett. **123**, 200601 (2019).
[12] P. Helms, U. Ray, and Garnet Kin-Lic Chan, Phys. Rev. E **100**, 022101 (2019).
[13] L. Causer, I. Lesanovsky, M. C. Bañuls, and J. P. Garrahan, Phys. Rev. E **102**, 052132 (2020).
[14] L. Causer, J. P. Garrahan, and A. Lamacraft, Phys. Rev. E **106**, 014128 (2022).
[15] J. Gu and F. Zhang, New J. Phys. **24**, 113022 (2022).
[16] L. Causer, M. C. Bañuls, and J. P. Garrahan, Phys. Rev. Lett. **128**, 090605 (2022).
[17] J. Eisert, M. Cramer, and M. B. Plenio, Rev. Mod. Phys. **82**, 277 (2010).
[18] T. Prosen and I. Pižorn, Phys. Rev. A **76**, 032316 (2007).
[19] F. Verstraete and J. I. Cirac, arXiv:cond-mat/0407066.
[20] P. Helms and Garnet Kin-Lic Chan, Phys. Rev. Lett. **125**, 140601 (2020).
[21] Y.-Y. Shi, L.-M. Duan, and G. Vidal, Phys. Rev. A **74**, 022320 (2006).
[22] N. E. Strand, H. Vroylandt, and T. R. Gingrich, J. Chem. Phys. **156**, 221103 (2022).
[23] N. E. Strand, H. Vroylandt, and T. R. Gingrich, J. Chem. Phys. **157**, 054104 (2022).
[24] D. Bauernfeind and M. Aichhorn, SciPost Phys. **8**, 024 (2020).
[25] J. Jäckle and S. Eisinger, Z. Phys. B **84**, 115 (1991).
[26] F. Ritort and P. Sollich, Adv. Phys. **52**, 219 (2003).
[27] L. Berthier and J. Garrahan, J. Phys. Chem. B **109**, 3578 (2005).
[28] C. Casert, T. Vieijra, S. Whitelam, and I. Tamblyn, Phys. Rev. Lett. **127**, 120602 (2021).
[29] K. Mallick, Physica (Amsterdam) **418A**, 17 (2015).
[30] See Supplemental Material at http://link.aps.org/supplemental/10.1103/PhysRevLett.130.147401 for more details, which includes Refs. [31–34].
[31] N. Schuch, M. M. Wolf, F. Verstraete, and J. I. Cirac, Phys. Rev. Lett. **98**, 140506 (2007).
[32] P. Corboz, R. Orús, B. Bauer, and G. Vidal, Phys. Rev. B **81**, 165104 (2010).
[33] H. N. Phien, J. A. Bengua, H. D. Tuan, P. Corboz, and R. Orús, Phys. Rev. B **92**, 035142 (2015).
[34] M. Suzuki, J. Math. Phys. (N.Y.) **26**, 601 (1985).
[35] C. Gardiner, *Handbook of Stochastic Methods* (Springer, Berlin, 2004).
[36] J. P. Garrahan, Physica (Amsterdam) **504A**, 130 (2018).
[37] H. Touchette, Phys. Rep. **478**, 1 (2009).
[38] H. Touchette, Physica (Amsterdam) **504A**, 5 (2018).
[39] R. L. Jack, Eur. Phys. J. B **93**, 74 (2020).
[40] J. P. Garrahan, R. L. Jack, V. Lecomte, E. Pitard, K. van Duijvendijk, and F. van Wijland, Phys. Rev. Lett. **98**, 195702 (2007).
[41] C. Maes, Phys. Rep. **850**, 1 (2020).
[42] M. Lubasch, J. I. Cirac, and M.-C. Bañuls, New J. Phys. **16**, 033014 (2014).

[43] M. Lubasch, J. I. Cirac, and M.-C. Bañuls, Phys. Rev. B **90**, 064425 (2014).
[44] The results are compared to those of 2D DMRG. They are considered quasi-exact, because by checking for covergence in the MPS bond dimension, we ensure high precision in the measured value, with an error which is orders of magnitude smaller than those of PEPS.
[45] H. C. Jiang, Z. Y. Weng, and T. Xiang, Phys. Rev. Lett. **101**, 090603 (2008).
[46] J. P. Garrahan, R. L. Jack, V. Lecomte, E. Pitard, K. van Duijvendijk, and F. van Wijland, J. Phys. A **42**, 075007 (2009).
[47] B. Derrida, J. Stat. Mech. (2007) P07023.
[48] T. Bodineau and B. Derrida, C. R. Acad. Sci. **8**, 540 (2007).
[49] C. Appert-Rolland, B. Derrida, V. Lecomte, and F. van Wijland, Phys. Rev. E **78**, 021122 (2008).
[50] V. Lecomte, J. P. Garrahan, and F. van Wijland, J. Phys. A: Math. Theor. **45**, 175001 (2012).
[51] R. L. Jack, I. R. Thompson, and P. Sollich, Phys. Rev. Lett. **114**, 060601 (2015).
[52] T. Nemoto, R. L. Jack, and V. Lecomte, Phys. Rev. Lett. **118**, 115702 (2017).
[53] D. Karevski and G. M. Schütz, Phys. Rev. Lett. **118**, 030601 (2017).
[54] L. Causer, M. C. Bañuls, and J. P. Garrahan, Data for 'optimal sampling of dynamical large deviations in two dimensions via tensor networks' (2022), 10.17639/nott.7238.
[55] V. S. Borkar, S. Juneja, and A. A. Kherani, Commun. Inf. Syst. **3**, 259 (2003).
[56] D. Simon, J. Stat. Mech. (2009) P07017.
[57] R. L. Jack and P. Sollich, Prog. Theor. Phys. Suppl. **184**, 304 (2010).
[58] R. Chetrite and H. Touchette, Ann. Henri Poincaré **16**, 2005 (2015).
[59] J. P. Garrahan, J. Stat. Mech. (2016) 073208.
[60] L. Causer, M. C. Bañuls, and J. P. Garrahan, Phys. Rev. E **103**, 062144 (2021).
[61] K. Ueda, R. Otani, Y. Nishio, A. Gendiar, and T. Nishino, J. Phys. Soc. Jpn. **74**, 111 (2005).
[62] M. Frías-Pérez, M. Mariën, D. Pérez-García, M. C. Bañuls, and S. Iblisdir, arXiv:2104.13264.
[63] M. M. Rams, M. Mohseni, D. Eppens, K. Jałowiecki, and B. Gardas, Phys. Rev. E **104**, 025308 (2021).
[64] T. Vieijra, J. Haegeman, F. Verstraete, and L. Vanderstraeten, Phys. Rev. B **104**, 235141 (2021).
[65] C. Giardina, J. Kurchan, and L. Peliti, Phys. Rev. Lett. **96**, 120603 (2006).
[66] F. Cérou and A. Guyader, Stoch. Anal. Appl. **25**, 417 (2007).
[67] V. Lecomte and J. Tailleur, J. Stat. Mech. (2007) P03004.
[68] T. Nemoto, F. Bouchet, R. L. Jack, and V. Lecomte, Phys. Rev. E **93**, 062123 (2016).
[69] U. Ray, G. K.-L. Chan, and D. T. Limmer, J. Chem. Phys. **148**, 124120 (2018).
[70] K. Klymko, P. L. Geissler, J. P. Garrahan, and S. Whitelam, Phys. Rev. E **97**, 032123 (2018).
[71] G. Ferré and H. Touchette, J. Stat. Phys. **172**, 1525 (2018).
[72] J. P. Garrahan and F. Pollmann, arXiv:2203.08200.
[73] P. G. Bolhuis, D. Chandler, C. Dellago, and P. L. Geissler, Annu. Rev. Phys. Chem. **53**, 291 (2002).
[74] Y. Tang, J. Liu, J. Zhang, and P. Zhang, arXiv:2208.08266.